Numerical simulation of fast depressurization using 4-equation and 6-equation models

Anil Gun, Yannick Hoarau, Eric Goncalves da Silva

NUMERICAL SIMULATION OF FAST DEPRESSURIZATION USING 4-EQUATION AND 6-EQUATION MODELS

A.K. Gun, Y. Hoarau
Department of Mechanics, Icube Laboratory, University of Strasbourg
1 Cr des Cigarières, 67000 Strasbourg, France
anil-kemal.gun@etu.unistra.fr, hoarau@unistra.fr

E. Goncalves
Department of Fluids, Thermal and Combustion, Institut Pprime, ISAE-ENSMA
86961 Chasseneuil cedex, France
eric.goncalves@ensma.fr

ABSTRACT

In the event of a Loss of Coolant Accident (LOCA) in a Pressurized Water Reactor (PWR), significant mass transfer and multiphase phenomena occur as the coolant rapidly vaporizes due to sudden depressurization. The transition from liquid to vapor, coupled with the dynamic movement of steam and liquid phases, interacts with pressure waves, impacting the reactor's thermal-hydraulic response. Accurately modeling these complex multiphase mass transfer processes is essential for predicting reactor behavior and ensuring the effective operation of emergency cooling systems, thereby enhancing reactor safety and reliability. In this study, we explore the numerical simulation of depressurization using 4-equation and 6-equation models.

1.INTRODUCTION

Numerical modeling of compressible two-phase flow plays a crucial role across various engineering disciplines, including the design of submarine and naval vehicles, as well as in the aerospace and nuclear power sectors. During regular operation, Pressurized Water Reactors maintain their coolant in a liquid state. However, during an accident, this coolant can transform into a combination of liquid and vapor phases. Since the 1960s, numerous predictive models for two-phase flow in nuclear thermal hydraulics have been developed and implemented in codes like RELAP, CATHARE, and ATHLET. The precision and complexity of these models and their associated simulations can differ due to the system's hyperbolic characteristics. A significant focus in nuclear thermal hydraulics has been to model the response of PWRs during LOCA, a common type of failure. In such scenarios, two primary physical processes are involved and interact: the movement of pressure waves and mass transfer. Understanding these processes is crucial for accurately predicting the system's behavior. Hence, there is an expectation that numerical models will provide detailed information about the mechanical forces exerted on the nuclear fuel and other components of the reactor. In the field of numerical analysis, the theoretical scenario often involves a coolant loss accident primarily occurring in the primary circuit's cold leg. A sudden pipe rupture in the primary circuit triggers rapid system depressurization. During this depressurization, the high-pressure coolant within the primary circuit encounters the containment structure's low-pressure environment, potentially generating a rarefaction wave that travels through the primary circuit and the Reactor Pressure Vessel (RPV). Initially, the depressurization wave propagates as a single-phase liquid flow, but after a few milliseconds, it shifts to a two-phase flow domain [1]. When the primary system pressure drops

to a certain threshold, the Emergency Core Cooling System (ECCS) injects a substantial volume of borated coolant water into the primary system. This action helps maintain the cladding temperature within permissible limits and ensures long-term cooling [2].

The literature presents a range of methods for simulating two-phase flow, ranging from complete models with seven-equation [3] to one-fluid homogeneous mixture model [4] [5]. In this study, we will explore the numerical solution for the rapid depressurization of CO_2 and water using the four-equation model [6], and the single velocity six-equation model [7]. Canon and Super-Canon experiments [8] which were conducted in the late 1970s, were simulated using these models. These tests were designed to evaluate the depressurization of heated water by simulating LOCA in a PWR primary circuit.

2.MATHEMATICAL MODEL

The single velocity six-equation model is composed of several key components: an advection equation for the volume fraction of one phase, separate mass and energy equations for each phase, and a single equation for the mixture's momentum. The six-equation model is based on the premise that velocity equilibrium between the two phases is achieved instantaneously. Despite this, the model still takes into account the differences in mechanical, thermal, and chemical equilibrium states. The model with stiff mechanical, thermal and chemical relaxation can be written in the following form in 1D :

$$\partial_t \alpha_1 + u\partial_x \alpha_1 = \mu(p_1 - p_2) + v(g_2 - g_1)/\rho_I \quad (1)$$

$$\partial_t(\alpha_1\rho_1) + \partial_x(\alpha_1\rho_1 u) = v(g_2 - g_1) \quad (2)$$

$$\partial_t(\alpha_2\rho_2) + \partial_x(\alpha_2\rho_2 u) = -v(g_2 - g_1) \quad (3)$$

$$\partial_t(\rho u) + \partial_x(\rho u^2 + \alpha_1 p_1 + \alpha_2 p_2) = 0 \quad (4)$$

$$\partial_t(\alpha_1 E_1) + \partial_x[\alpha_1(E_1 + p_1)u] + \Sigma(U, \partial_x U) = -\mu p_I(p_1 - p_2) + \theta(T_2 - T_1) + e_I v(g_2 - g_1) \quad (5)$$

$$\partial_t(\alpha_2 E_2) + \partial_x[\alpha_2(E_2 + p_2)u] - \Sigma(U, \partial_x U) = \mu p_I(p_1 - p_2) - \theta(T_2 - T_1) - e_I v(g_2 - g_1) \quad (6)$$

where α_k is the volume fraction of phase k, $k = 1, 2$, and saturation condition is assumed ($\alpha_1 + \alpha_2 = 1$), p_k is the phasic pressure, and ρ_k is the phasic density. Phasic total energy denoted as $E_k = \mathcal{E}_k + \frac{1}{2}\rho_k u^2$, where $\mathcal{E}_k = \rho_k \varepsilon_k$ is the phasic internal energy, with phasic specific internal energy ε_k. The right-hand side represents the pressure, thermal and chemical relaxation process, where μ, θ and v represent the parameters for mechanical, thermal and chemical relaxation, respectively. For pressure relaxation process, where $p_I = \frac{Z_2 p_1 + Z_1 p_2}{Z_1 + Z_2}$ represent the interface pressure, and $Z_k = \rho_k c_k$ is the acoustic impedance, and c_k is the sound of speed of the phase k. It is assumed that mechanical relaxation occurs instantaneously which means that $\mu \to +\infty$. Regarding the interfacial density ρ_I and the interfacial specific total energy e_I, due to the handling of thermal and chemical source terms, specifying these expressions is unnecessary. At certain designated locations, it is presumed that these parameters ($\theta \to +\infty$, $v \to +\infty$) have infinite values, whereas elsewhere they are set to zero. Specifically, thermal transfer occurs at liquid-vapor interfaces, and thermo-chemical transfer is activated at liquid-vapor interfaces in metastable thermodynamic conditions. The phasic total energy equations contain nonconservative terms :

$$\Sigma(U, \partial_x U) = -u[Y_2 \partial_x(\alpha_1 p_1) - Y_1 \partial_x(\alpha_2 p_2)] \quad (7)$$

where $Y_k = \alpha_k \rho_k / \rho$. It is crucial to highlight that combining the two nonconservative phasic total energy equations yields the equation that expresses the conservation of the mixture's total energy $E = \mathcal{E} + \frac{1}{2}u^2 = \alpha_1 E_1 + \alpha_2 E_2$.

$$\partial_t(E) + \partial_x[(E + \alpha_1 p_1 + \alpha_2 p_2)u] = 0 \quad (8)$$

A four-equation model is employed to depict a two-phase flow in kinetic, mechanical, and thermal equilibrium. This model is derived from the seven-equation Baer-Nunziato two-phase model [3], under the conditions of velocity, pressure, and temperature equilibrium. It includes one mass equation for each phase, along with momentum and energy equations for the mixture. Four-equation model can be written in the following form in 1D :

$$\partial_t(\alpha_1\rho_1) + \partial_x(\alpha_1\rho_1 u) = v(g_2 - g_1) \tag{9}$$
$$\partial_t(\alpha_2\rho_2) + \partial_x(\alpha_2\rho_2 u) = -v(g_2 - g_1) \tag{10}$$
$$\partial_t(\rho u) + \partial_x(\rho u^2 + p) = 0 \tag{11}$$
$$\partial_t(E) + \partial_x[(E+p)u] = 0 \tag{12}$$

In this context, ρ_k represents the phasic density, while α_k ($\alpha_1 + \alpha_2 = 1$) denotes the volume fraction, for each respective phase. Additionally, ρ, u, P, and E ($E = \mathcal{E} + \frac{1}{2}\rho u^2$) denotes mixture velocity, density, pressure, and total energy respectively. The right-hand side depicts mass transfer, with g_l and g_v representing the chemical potentials (Gibbs free energy) of the gaseous and liquid phases.

A fundamental requirement for fully describing and closing a physical system is an equation of state that correlates temperature, pressure, internal energy, and density. A stiffened gas equation of state (SG EoS) is selected for this purpose :

$$p_k(\mathcal{E}_k, \rho_k) = (\gamma_k - 1)(\mathcal{E}_k - \rho_k q_k) - \gamma_k p_{\infty,k}, \qquad T_k(p_k, \rho_k) = \frac{p_k + p_{\infty,k}}{\rho_k C_{v,k}(\gamma_k - 1)} \tag{13}$$

$$h_k(p_k, T_k) = C_{p,k}T + q, \qquad \varepsilon_k(p_k, T_k) = \frac{(p_k + \gamma_k p_{\infty,k})C_{v,k}T_k}{p_k + p_{\infty,k}} + q_k \tag{14}$$

According to the aforementioned relationships, the specific entropy (s_k), and Gibbs free energy (g_k), for each phase are determined :

$$s_k(p_k, T_k) = C_{v,k} \ln \frac{T_k^{\gamma_k}}{(p_k + p_{\infty,k})^{\gamma - 1}} + q' \tag{15}$$

$$g_k(p_k, T_k) = (\gamma_k C_{v,k} - q')T_k - C_{v,k}T_k \ln \frac{T_k^{\gamma_k}}{(p_k + p_{\infty,k})^{\gamma - 1}} + q \tag{16}$$

where $\gamma = \frac{C_p}{C_v}$ is the heat capacity ratio, C_p and C_v are thermal capacities, and P_∞, q, and q' are characteristic constants of the thermodynamic behavior of the fluid. Considering the four-equation model, the mixture pressure and temperature can be defined as [6] :

$$p = \frac{-a_1 + \sqrt{a_1^2 - 4a_0a_2}}{2a_2}, \qquad T = (e - q^*)\left(\sum \frac{Y_k C_{vk}(p_k + \gamma_i p_{\infty,k})}{p_k + p_{\infty,k}}\right)^{-1} \tag{17}$$

$$a_2 = Y_1 C_{v1} + Y_2 C_{v2} \tag{18}$$

$$a_1 = Y_1 C_{v1}(p_{\infty,2} + \gamma_1 p_{\infty,1} - (\gamma_1 - 1)Q) + Y_2 C_{v2}(p_{\infty,1} + \gamma_2 p_{\infty,2} - (\gamma_2 - 1)Q) \tag{19}$$

$$a_0 = -Q((\gamma_1 - 1)Y_1 C_{v1} p_{\infty,2} + (\gamma_2 - 1)Y_2 C_{v2} p_{\infty,1})) + p_{\infty,1}p_{\infty,2}(\gamma_1 Y_1 C_{v1} + \gamma_2 Y_2 C_{v2}) \tag{20}$$

where $q^* = Y_1 q_1 + Y_2 q_2$, and $Q = \rho(e - q^*)$.

The fractional step method [9] has been employed to solve both the 4-equation and 6-equation models. In the first step, the homogeneous part of the system is solved without the source term. The solution from this initial step is then used in the subsequent relaxation step. The

homogeneous part of the system is solved using the Harten-Lax-van Leer Contact (HLLC) approximate Riemann solver [10]. The process can be summarized as follows :

$$U_i^{n+1} = L_{hyp}^{\Delta t} L_{source}^{\Delta t} U_i^n \tag{21}$$

After solving the homogeneous system, a sequence of ordinary differential equation systems is solved, taking into account the relaxation source terms. During any relaxation process, the mixture density, velocity, total energy, and internal energy remain constant throughout the transfer processes. Furthermore, in the absence of activated chemical relaxation, the partial densities also remain constant. (For an in-depth discussion on the mechanical and thermal relaxation processes, refer to reference [7].)

The theoretical pressure-temperature saturation curve for liquid and vapor phases is established by satisfying the Gibbs free energy equilibrium condition, where the Gibbs free energies of the two phases, g_1 and g_2, are set equal. Using the SG EoS equations, the pressure-temperature saturation curve is characterized by the following equation :

$$A_s + \frac{B_s}{T} + C_s lnT + D_s ln(p + p_{\infty,1}) - ln(p + p_{\infty,2}) = 0 \tag{22}$$

with

$$A_s = \frac{C_{p1} - C_{p2} + q_2^{'} - q_1^{'}}{C_{p2} - C_{v2}}, B_s = \frac{q_2 - q_1}{C_{p2} - C_{v2}}, C_s = \frac{C_{p2} - C_{p1}}{C_{p2} - C_{v2}}, D_s = \frac{C_{p1} - C_{v1}}{C_{p2} - C_{v2}} \tag{23}$$

By employing the above non-linear formula, the saturation temperature corresponding to the pressure can be determined. After the chemical relaxation, equilibrium pressure (p^{***}), temperature (T^{***}), partial densities (ρ_k^{***}), and volume fraction (α^{***}) for infinite-rate relaxation ($v \to +\infty$) :

$$a_2(p^{***})(T^{***})^2 + a_1(p^{***})(T^{***}) + a_0(p^{***}) = 0 \tag{24}$$

$$a_2(p^{***}) = \rho^0 C_{v1} C_{v2}((\gamma_2 - 1)(p^{***} + \gamma_1 p_{\infty,1}) - (\gamma_1 - 1)(p^{***} + \gamma_2 p_{\infty,2})) \tag{25}$$

$$\begin{aligned} a_1(p^{***}) = {} & \mathcal{E}^0((\gamma_1 - 1)C_{v1}(p^{***} + p_{\infty,2}) - (\gamma_2 - 1)C_{v2}(p^{***} + p_{\infty,1})) + \\ & \rho^0((\gamma_2 - 1)C_{v2}q_1(p^{***} + p_{\infty,1}) - (\gamma_1 - 1)C_{v1}q_2(p^{***} + p_{\infty,2})) \\ & C_{v2}(p^{***} + p_{\infty,1})(p^{***} + \gamma_2 p_{\infty,2}) - C_{v1}(p^{***} + p_{\infty,2})(p^{***} + \gamma_1 p_{\infty,1}) \end{aligned} \tag{26}$$

$$a_0(p^{***}) = (q_2 - q_1)(p^{***} + p_{\infty,1})(p^{***} + p_{\infty,2}) \tag{27}$$

$$T^{***}(p^{***}) = \frac{-a_1(p^{***}) + \sqrt{a_1(p^{***})^2 - 4a_0(p^{***})a_2(p^{***})}}{2a_2(p^{***})} \tag{28}$$

$$\rho_k^{***} = \frac{p^{***} + p_{\infty,k}}{(\gamma_k - 1)C_{vk}T^{***}} \qquad \alpha_1^{***} = \frac{\rho^0 - \rho_2^{***}}{\rho_1^{***} - \rho_2^{***}} \tag{29}$$

Although the steps of chemical relaxation for the 6-equation model are expressed here, it can be used in the 4-equation model.

Moreover, chemical relaxation, defined as an infinite rate, can be modeled by the evolution of the mass fraction of vapor through the following differential equation [11] :

$$\frac{DY_{vap}}{Dt} = -\frac{Y_{vap} - Y_{vap}^{***}}{\Theta} \tag{30}$$

$$Y_{vap}^{n+1} = Y_{vap}^{***} - (Y_{vap}^{***} - Y_{vap}^{n})exp^{-\Delta t/\Theta} \tag{31}$$

$$\Theta = \Theta_0 \alpha_v^{-0.54} [\frac{P_S(T_{in}) - P}{P_{crit} - P_S(T_{in})}]^{-1.76} \tag{32}$$

where $\Theta_0 = 3.84$ x 10^{-7} s [12], $P_s(T_{in})$ saturation pressure corresponding to the initial temperature, and P_{crit} is the critical pressure (22.064 MPa). This type of mass transfer will be tested in a 4-equation model. It is designated as 4-eqt-DZ2.

3.RESULTS

The first test case was proposed by Lund [13], involving the depressurization of a pipe filled with CO_2. The total length of the pipe is 80 meters, with the initial discontinuity set at 50 meters. The initial conditions are as follows: on the left side, the pressure P_L is 60 bar, the temperature T_L is 273 K, and the volume fraction is $\alpha_L = 1 \times 10^{-5}$; on the right side, the pressure P_R is 10 bar, the temperature T_R is 273 K, and the volume fraction is $\alpha_R = 1 - \alpha_L$. The parameters for the equation of state are presented in Table 1.

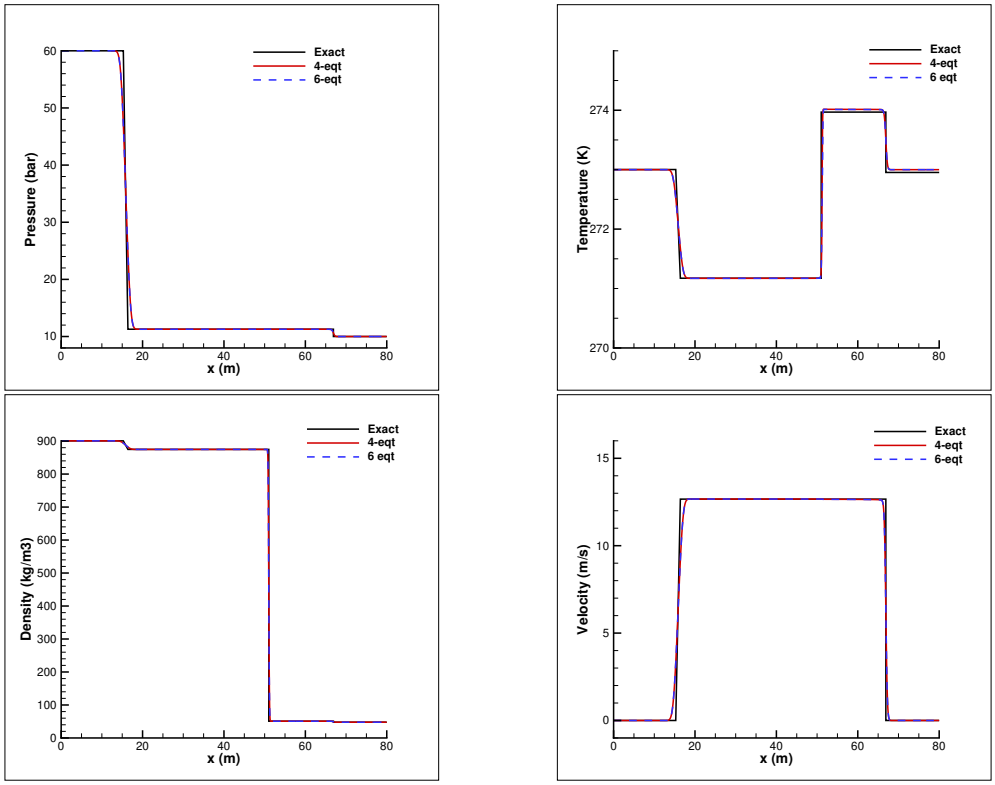

Figure 1 - Results of CO_2 pipe depressurization for pressure, temperature, density, and velocity at t= 0.08 s, without mass transfer.

Table 1 - EoS parameters for CO_2 test case.

	Liquid	Vapor
γ	1.23	1.06
P_∞ (Pa)	1.32×10^8	8.86×10^5
q (J.kg^{-1})	-6.23×10^5	-3.01×10^5
C_v (J.kg^{-1}.K^{-1})	2.44×10^3	2.41×10^3
q' (J.kg^{-1}.K^{-1})	-5.34×10^3	-1.03×10^4

For the CO_2 depressurization test case, simulations were conducted with and without mass transfer using a 5000-cell mesh. The results at t = 0.08 s are presented in Figures 1 and 2,

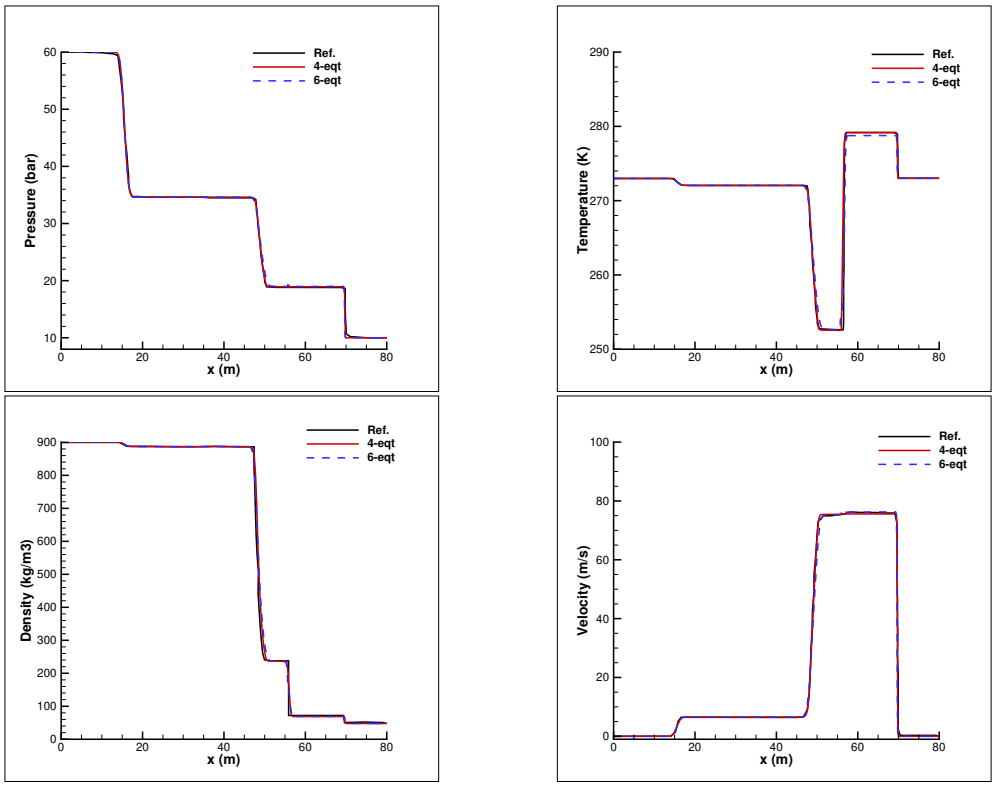

Figure 2 - Results of CO_2 pipe depressurization for pressure, temperature, density, and velocity at t= 0.08 s, with mass transfer.

respectively. In the first scenario without mass transfer (Fig. 1), the density profile consists of three waves: an expansion wave on the left, a shock wave on the right, and an initial contact discontinuity at $x = 50\,\text{m}$. In the second scenario with mass transfer (Fig. 2), we observe that thermochemical transfer is activated at liquid-vapor interfaces under metastable thermodynamic conditions ($T_{liq} > T_{sat}$). The temperature variation caused by the liquid-to-vapor transition generates a new wave between the initial discontinuity and the right section of the pipe. The outcomes from both scenarios show good agreement with the reference results.

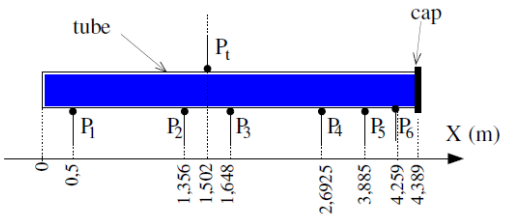

Figure 3 - Schematic of experiment facility.

The Canon and Super-Canon experiments were established to replicate a full-scale LOCA within a PWR primary circuit. This involved creating a complete break, leading to the rapid depressurization of a horizontal pipe. As can be seen in Figure 3, the experimental tube has a length of 4.389 m and an internal diameter of 102.3 mm, sealed at one end and initially containing undersaturated water. Upon rupturing the membrane at the other end, a rarefaction wave is initiated, moving through the tube. Although void fraction measurements are taken at a single point, pressure data is collected at multiple locations along the tube. For the Canon

experiment, the initial pressure and temperature of the pipe were set to 32 bar and 220°C, respectively. For the Super-Canon experiment, these values were set to 150 bar and 300°C. The pressure and temperature of the experimental environment were 1 bar and ambient temperature. However, in the numerical simulation, this part was filled with vapor instead of air at 1 bar, with temperatures of 220°C for the Canon experiment and 300°C for the Super-Canon experiment.

Table 2 - EoS parameters for liquid and vapor for the Canon & Super-Canon experiment.

	Liquid	Vapor
γ	1.66	1.34
P_∞ (Pa)	769317123.86	0.00
q (J.kg^{-1})	-1359570.00	2032350.00
C_v (J.kg^{-1}.K^{-1})	2807.61	1162.00
q' (J.kg^{-1}.K^{-1})	11671.61	2351.11

Table 3 - Initial conditions for the Canon (left) & Super-Canon (right) experiment

	Pipe	Tank		Pipe	Tank
α_l	$1-10^{-3}$	10^{-3}	α_l	$1-10^{-3}$	10^{-3}
α_v	10^{-3}	$1-10^{-3}$	α_v	10^{-3}	$1-10^{-3}$
ρ_l (kg.m^{-3})	841.12	837.74	ρ_l (kg.m^{-3})	736.45	717.72
ρ_v (kg.m^{-3})	16.72	0.52	ρ_v (kg.m^{-3})	88.23	0.59
P_l (bar)	32	1	P_l (bar)	150	1
P_v (bar)	32	1	P_v (bar)	150	1

Numerical simulations have been simulated using a 1D simplified geometry with 1000 cells mesh, and closed-end as a boundary condition on one side and atmospheric pressure tank other side. In addition, the computational domain is determined as 10 m. The stiffened gas EoS and initial conditions given in the table 2 and 3. As can be seen in Figure 4, the experimental results are labeled as 'Exp.' The 4-equation model results, which include mechanical, thermal, and chemical relaxation, are labeled as '4-eqt-pTg.' The non-instantaneous chemical relaxation model is labeled as '4-eqt-DZ2.' Additionally, the 6-equation model results, which include mechanical and thermal relaxation, are labeled as '6-eqt-pT,' while the version that includes mechanical, thermal, and chemical relaxation is labeled as '6-eqt-pTg. In addition, the results obtained from the solver have been compared with data from the literature (HRM Tabulated EoS legend [14]). The initial depressurization is both abrupt and rapid. The pressure falls below the saturation pressure corresponding to the initial stagnation temperature, which is 23.2 bar for Canon and 85.8 bar for Super-Canon. This causes the liquid water to penetrate into the metastable region. The primary events during the experiment can be summarized as follows: the sudden onset of depressurization generates a rarefaction wave that propagates leftward through the tube. As the rarefaction wave rapidly propagates, leading to vaporization at a relatively constant pressure for a time. After this period, the pressure continues to decrease until it reaches the atmospheric pressure. Importantly, differences were found between the experimental results and the computational predictions, with the computations indicating an earlier start of vaporization compared to what was observed in the experiments.

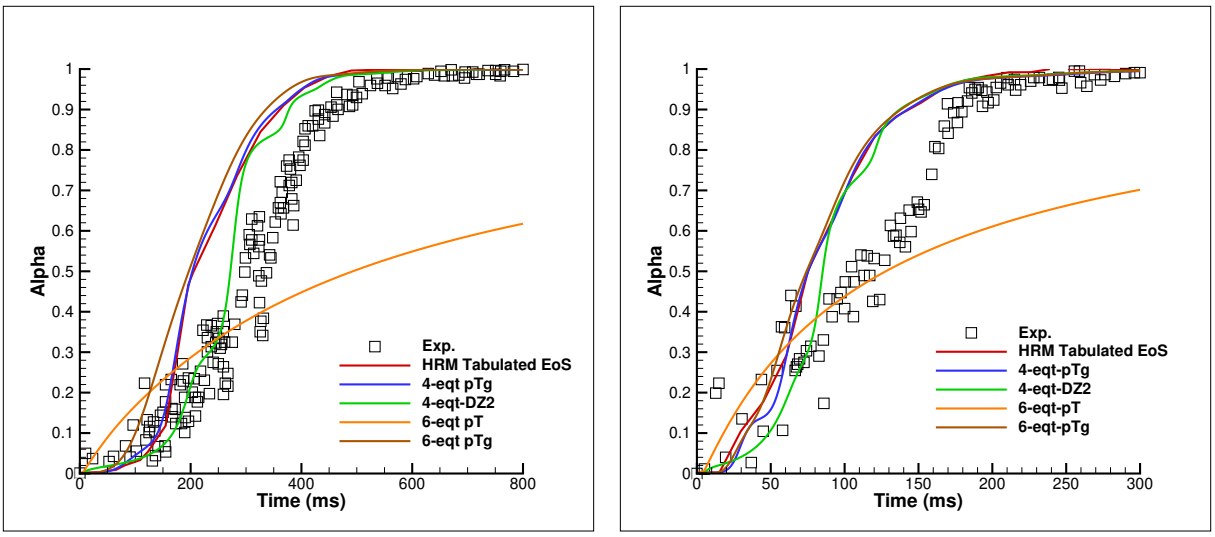

Figure 4 - Vapor void fraction versus time at the PT location, comparing Canon (left) and Super-Canon (right) experiments.

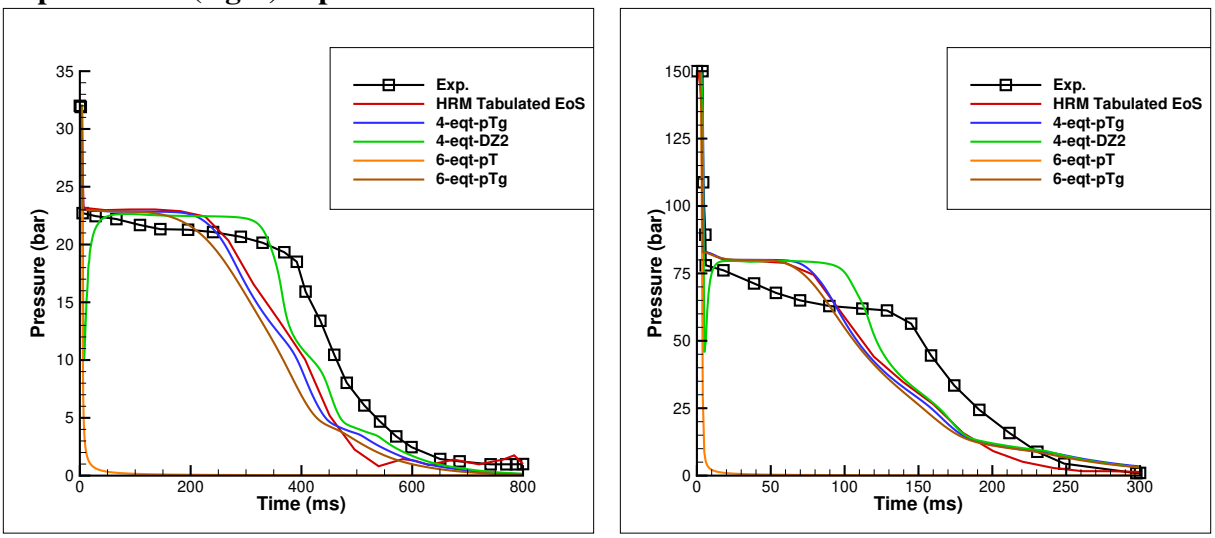

Figure 5 - Pressure versus time at the P1 location, comparing Canon (left) and Super-Canon (right) experiments.

4.CONCLUSION

In this study, the CO_2 test case and Canon & Super-Canon experiments were simulated using 4-equation and 6-equation models. The results obtained for the depressurization of CO_2 align well with the reference results. However, it is important to note that, for the Canon & Super-Canon experiments, computational vaporization was predicted to occur earlier than observed in the actual experiments. Within the wide range of pressures and temperatures considered in this study, the stiffened gas equation of state appears overly simplistic for accurately capturing the thermodynamic characteristics of water. Nevertheless, a reasonable level of agreement is observed between the results obtained using the 4-equation and 6-equation models, demonstrating the effectiveness of the current models in replicating the experimental data, even in complex and challenging numerical scenarios.

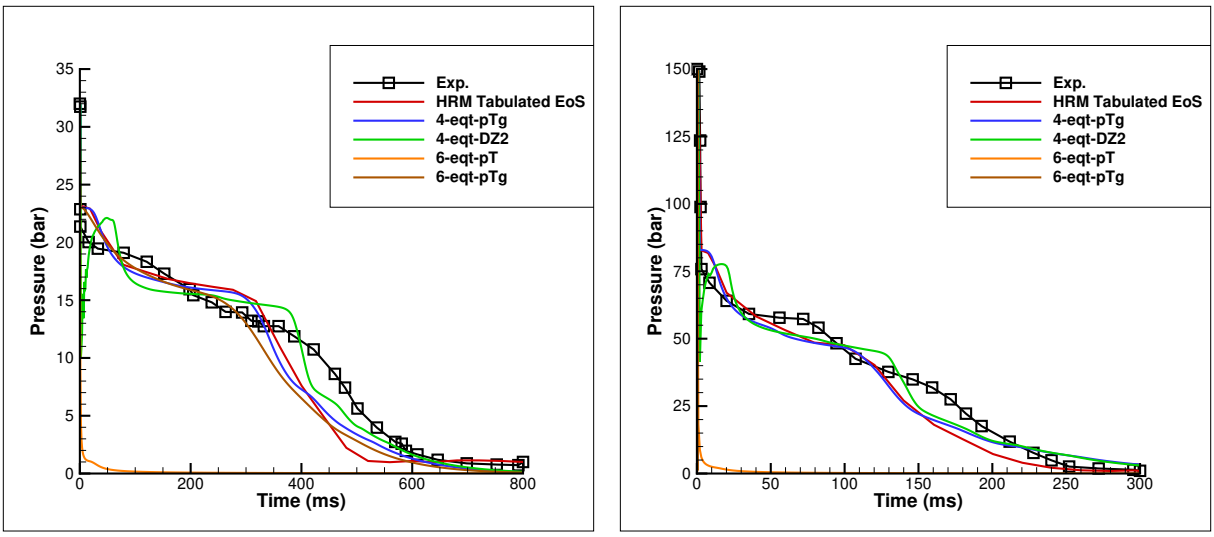

Figure 6 - Pressure versus time at the P5 location, comparing Canon (left) and Super-Canon (right) experiments.

REFERENCES

1. Faucher, V., Crouzet, F., Piteau, P., Galon, P., & Izquierdo, P. (2012). Numerical and experimental analysis of transient wave propagation through perforated plates for application to the simulation of LOCA in PWR. *Nuclear engineering and design*, 253, 1-11

2. Tong, L. S., & Weisman, J. (1979). Thermal analysis of pressurized water reactors.

3. Baer, M.R., and Nunziato, J.W. (1986) A two-phase mixture theory for the deflagration-to-detonation transition (DDT) in reactive granular materials. *Int. J. Multiph. Flow.* 12, 861–889

4. Goncalves, E., & Patella, R. F. (2009). Numerical simulation of cavitating flows with homogeneous models. *Computers & Fluids*, 38(9), 1682-1696.

5. Goncalves, E., & Hoarau, Y. (2022). Mass transfer modelling for compressible two-phase flows. *In AIP Conference proceeding, ICNAAM Symposium*, 19-23 September 2022, Grece.

6. Saurel, R., Boivin, P., and Le Métayer, O. (2016). A general formulation for cavitating, boiling and evaporating flows. *Computers Fluids,* 128, 53-64.

7. Pelanti, M. and Shyue, K. (2014) A mixture-energy-consistent six-equation two-phase numerical model for fluids with interfaces, cavitation and evaporation waves. *J. Comput. Phys.* 259, 331–357

8. Riegel, B. (1978) Contribution à l'étude de la décompression d'une capacité en régime diphasique. *L'institut National Polytechnique de Grenoble* PhD Thesis

9. LeVeque, R. J. (2002). Finite volume methods for hyperbolic problems (Vol. 31). Cambridge University Press.

10. Toro, E. F., Spruce, M., and Speares, W. (1994). Restoration of the contact surface in the HLL-Riemann solver. *Shock waves*, 4, 25-34.

11. De Lorenzo, M., Lafon, P., Di Matteo, M., Pelanti, M., Seynhaeve, J. M., & Bartosiewicz, Y. (2017). Homogeneous two-phase flow models and accurate steam-water table look-up method for fast transient simulations. *International journal of multiphase flow*, 95, 199-219.

12. Downar-Zapolski, P., Bilicki, Z., Bolle, L., and Franco, J. (1996). The non-equilibrium relaxation model for one-dimensional flashing liquid flow. *International journal of multiphase flow*, 22(3), 473-483.

13. Lund, H., & Aursand, P. (2012). Two-phase flow of CO2 with phase transfer. Energy Procedia, 23, 246-255.

14. Lepareux, M. (1994). Programme PLEXUS matériau eau modèle homogène équilibre. *Rapport* DMT, 94, 398.